Clinical Oral Investigations
https://doi.org/10.1007/s00784-018-2385-2

ORIGINAL ARTICLE

Bone mineralization and vascularization in bisphosphonate-related osteonecrosis of the jaw: an experimental study in the rat

Jean-Daniel Kün-Darbois[1,2] · Hélène Libouban[1] · Guillaume Mabilleau[1,3] · Florence Pascaretti-Grizon[1] · Daniel Chappard[1,3]

Received: 12 April 2017 / Accepted: 7 February 2018

Abstract

Objectives Pathogenesis of bisphosphonate-related osteonecrosis of the jaws (BRONJ) is not fully explained. An antiangiogenic effect of bisphosphonates (BPs) or an altered bone quality have been advocated. The aims of the present study were to analyze alveolar mandibular vascularization and bone quality in rats with BRONJ.

Materials and methods Thirty-eight Sprague-Dawley rats were randomized into two groups: zoledronic acid (ZA), $n = 27$, and control (CTRL) $n = 11$. The ZA group received a weekly IV injection of ZA (100 μg/kg) during 10 weeks. The CTRL group received saline. After 6 weeks, extraction of the right mandibular molars was performed. Rats were sacrificed after 14 weeks. Microtomography characterized bone lesions and vascularization after injection of a radio-opaque material. Raman microspectroscopy evaluated bone mineralization.

Results Fifty-five percent of ZA rats presented bone exposure and signs of BRONJ. None sign was found at the left hemimandible in the ZA group and in the CTRL group. Vascular density appeared significantly increased in the right hemimandibles of the CTRL group compared to the left hemimandibles. Vascularization was reduced in the ZA group. A significantly increased of the mineral-to-amide ratio was found in the alveolar bone of ZA rats by Raman microspectroscopy.

Conclusions In a rat model of BRONJ, microtomography evidenced osteonecrosis in BRONJ. Raman spectroscopy showed an increased mineralization. Vascularization after tooth extraction was impaired by ZA.

Clinical relevance Prolonged BP administration caused an increase in the mineralization and a quantitative reduction of the vascularization in the alveolar bone; both factors might be involved concomitantly in the BRONJ pathophysiology.

Keywords Bisphosphonate · BRONJ · Rat model · Osteonecrosis · Vascularization · Raman microspectroscopy · Microtomography

Introduction

Bisphosphonates (BPs) are structural analogs of inorganic pyrophosphate, and they are resistant to enzymatic hydrolysis. They have a strong affinity for the hydroxyapatite crystal and can remain several years in bone. They inhibit bone resorption by interfering with the mevalonate pathway in the osteoclast [1]. A large number of studies have confirmed their interest in reducing the incidence of osteoporosis-related fractures by increasing bone mineral density (BMD) [2, 3]. In human, intravenous amino-BPs injections are used in several indications such as osteoporosis, bone metastases, multiple myeloma, or hypercalcemia associated with an increased osteoclast number [4, 5].

Antiresorptive drug-related osteonecrosis of the jaw (ARONJ) is a major adverse event due to antiresorptive treatments and was first described with BP [6–9]. It is clinically defined as an area of exposed bone of the jaws that do not heal within 8 weeks after identification in a patient with an antiresorptive drug history and without irradiation therapy to the craniofacial region [10, 11]. The incidence of

✉ Daniel Chappard
daniel.chappard@univ–angers.fr

[1] Groupe d'Etude Remodelage Osseux et bioMatériaux GEROM, SFR 42-08, IRIS-IBS Institut de Biologie en Santé, Université d'Angers, CHU d'Angers 4, rue Larrey, 49933 Angers Cedex, France

[2] Service de chirurgie maxillo-faciale et stomatologie, CHU d'Angers, 4, rue Larrey, 49933 Angers Cedex, France

[3] SCIAM Service Commun d'Imagerie et Analyses Microscopiques, IRIS-IBS Institut de Biologie en Santé, Université d'Angers, CHU d'Angers 4, rue Larrey, 49933 Angers Cedex, France

Published online: 16 February 2018

bisphosphonate-related osteonecrosis of the jaw (BRONJ) ranges between 1% and 10% in patients undergoing IV BP therapy [12, 13]. The highest risk is in patients with multiple myeloma receiving iv zoledronic acid (ZA) treatment [14]. BRONJ is more often located at the mandible (70%) than at the maxilla (30%) [15]. A triggering factor with bone exposure (mainly consisting in tooth extractions) is found in the majority of cases [10, 15–18]. A BP therapy is often considered as a contraindication to dental implant treatment [19–21].

The pathogenesis of BRONJ seems multifactorial but is not fully explained yet [22–24]. An explanation could be an impairment of jaw bone vascularization due to an antiangiogenic effect of BPs [25–29]. The role of bone quality with an increased stiffness of the bone matrix, due to a uniformity of the mineralization degree, has also been advocated [30]. Another explanation could be a direct toxicity of BPs for epithelial cells combined with a reduced microcirculation of the gingiva [22, 31]. The development of chronic osteomyelitis due to a contamination with *Actynomyces* is reported [22, 32].

An animal model mimicking the clinical features of BRONJ may help to understand the pathophysiological mechanisms of BRONJ and evaluate new treatments. Several models have been described in laboratory animals, but none of them reproduce strictly the clinical characteristics observed in the human disease [33–36].

The aims of the present study were to provoke BRONJ in the rat and to analyze the mandibular vascularization after intravascular injection of a radio-opaque material. The quality of the bone material was also assessed by Raman microspectrometry and quantitative backscattered electron imaging (qBEI) to evaluate the mineralization degree of the bone matrix.

Material and methods

Animals and experimental procedure

Animal care and experimental protocols were approved by the French Ministry of Research and were done in accordance with the institutional guidelines of the French Ethical Committee (protocol agreement number 01857.01), the European Communities Council Directive of 24 November 1986 (86/609/EEC) and under the supervision of authorized investigators. The flowchart of the study appears in (Fig. 1). Fifteen-week-old male Sprague-Dawley rats ($n = 38$), weighing 486.3 ± 10.8 g, were used for the study (Janvier-Labs, Le Genest-Saint-Isle, France). They were acclimated for 2 weeks to the local vivarium conditions (24 °C and 12 h/12 h light dark cycle) where they were given standard laboratory food (UAR, Villemoison-sur-Orge, France) and water ad libitum. Rats were randomized into two groups: a control group (CTRL, $n = 11$) and a zoledronic acid group (ZA, $n = 27$). Rats from the ZA group were anesthetized with isoflurane and injected intravenously with ZA (Zometa®, Novartis Pharma GmbH, Nuremberg, Germany) at a dose of 100 μg/kg, once a week, during 10 weeks. Injections were performed in a tail vein. Each animal of the ZA group received a total dose of ZA of 1000 μg/kg at the end of the protocol. Rats of the CTRL group were similarly injected with equivalent volume of saline solution. At sixth week, extractions of the three right mandibular molars were performed in rats of both group (see below). Rats were weighted weekly and sacrificed 14 weeks after the first injection by CO_2 inhalation. Visual examination of mandibular molar regions was performed in order to look for exposed bone. Rats were then randomized in two subgroups: subgroup A and subgroup B. $CTRL_A$ and ZA_A groups were used for micro-CT, Raman microspectrometry, and qBEI analysis; $CTRL_B$ and ZA_B

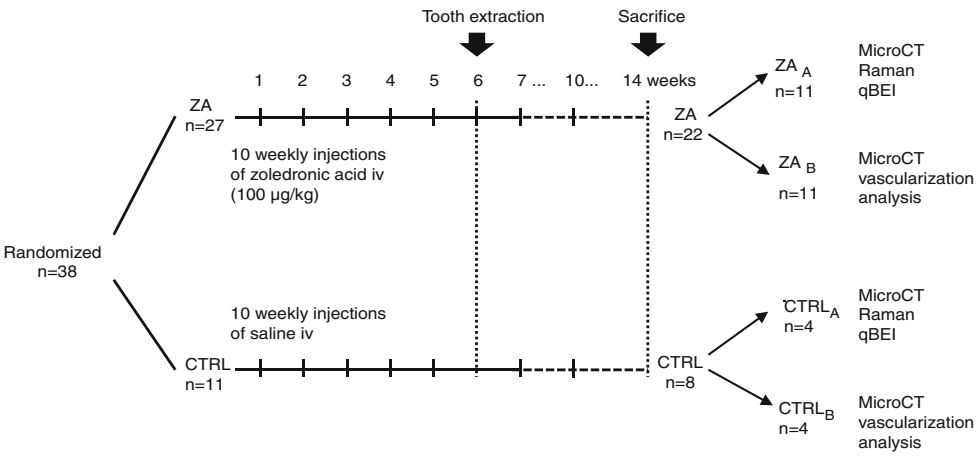

Fig. 1 Flowchart of the study showing animal repartitions in control group (CTRL) and zoledronic acid group (ZA) and in subgroup A ($CTRL_A$ and ZA_A) and subgroup B ($CTRL_B$ and ZA_B)

groups were injected with barium sulfate for vascularization analysis. Hemimandibles were then dissected, defleshed, and fixed in formalin during 24 h and transferred in absolute acetone.

Tooth extractions

Extraction of the molars was done as follows. General anesthesia was induced by intraperitoneal injection of 100 mg/kg ketamine (Renaudin, Aïnhoa, France) and 10 mg/kg xylazine (Rompun® 2%, Bayer, Leverkusen, Germany). Analgesia was obtained using subcutaneous injections of buprenorphine (Vetergesic®, Sogeval, Laval, France) at a dose of 0.03 mg/kg, half an hour before surgical procedure and postoperatively if needed. Tooth extraction was performed using rodent specific instrumentation (Coveto, Montaigu, France). Adequate exposure was obtained using a mouth gag and rodent cheek dilator with lingual traction. Each tooth was removed progressively using a Crossley molar luxator and a molar extractor. The first molar was separated into two halves with the luxator before removing. If needed, hemostasis was obtained with simple compression and no suture was done. No additional drug and no antibiotic was given. Rats were closely monitored until awakening.

Microcomputed tomography

Micro-CT of the right and left hemimandibles was performed using a Skyscan 1172 X-ray computerized microtomograph (Bruker microCT, Kontich, Belgium) equipped with an X-ray tube working at 70 kV/100 μA. Bones were placed in Eppendorf's tubes filled with water to prevent desiccation. The tubes were fixed on a brass stub with plasticine. Analysis was done with a pixel size corresponding to 10.5 μm; the rotation step was fixed at 0.25° and exposure was done with a 0.5-mm aluminum filter. For each hemimandible, a stack of 2D sections was obtained and reconstructed using NRecon software (Bruker) and analyzed with CTan software (Skyscan, release 1.13.11.0). Frontal, axial, and sagittal sections of alveolar regions were then obtained from 3D models using a surface-rendering program (Ant, release 2.0.5, Skyscan, Belgium). Three-dimensional reconstructions were obtained using CTVox software (Skyscan, release 2.5).

Raman microspectroscopic analysis

The left hemimandibles were used to evaluate bone quality at the alveolar bone where no tooth extraction had been done. Bone samples were immersed in sodium hypochlorite (50% in water) to remove organic tissues, rinsed 4 times in ultrapure water, and dried at room temperature. They were then polished on a grinding machine (Struers, Copenhagen, Denmark) using ascending grads of polishing paper (1200, 2000, and 4000) during 2 min each to expose the alveolar bone and the teeth roots. Bones were affixed onto glass slides with a hand press to obtain a horizontal surface parallel to the slide. Raman analyses were performed on a Senterra microscope with the OPUS 5.5 software (Bruker optic, Ettlingen, Germany). The excitation laser wavelength was 785 nm with an excitation power of 50 mW and 8–12 cm^{-1} spectral resolution to avoid the autofluorescence of the collagen. For each sample, the final spectrum was obtained by averaging 20 scans of 40 s. Average Raman spectra were obtained for control alveolar bone; ZA impregnated alveolar bone and dehydrated ZA from all rats from group A. An automatic baseline was applied, and four physicochemical parameters were determined from spectra [37]:

- Mineralization (mineral to matrix ratio) is the intensity ratio between the ν_1PO_4 (960 cm^{-1}) peak to the matrix bands (amide I 1667 cm^{-1} or amide III 1243 cm^{-1}).
- Carbonate substitution is the intensity ratio between B-type CO_3^{2-} (1071 cm^{-1}) band and the ν_1PO_4 (960 cm^{-1}) band.
- Relative proteoglycan (PG) content is the ratio of GAG/CH_3 (1365–1390 cm^{-1}) to the amide III band.
- Crystallinity is the inverse of the full width at half maximum intensity of the ν_1PO_4 band (960 cm^{-1}).

ZA spectrum was obtained from a sample of dehydrated ZA using the same procedure.

Quantitative backscattered electron imaging and energy-dispersive X-ray spectroscopy

Quantitative backscattered electron imaging was employed to determine the bone mineral density distribution (BMDD) in the same regions of alveolar bone as Raman analysis as previously reported. This methodology has been described in full details elsewhere [38, 39]. Bone samples were embedded undecalcified in poly (methylmethacrylate), and the blocks were polished to a 0.5-μm finish with diamond particles, carbon-coated, and observed with a scanning electron microscope (EVO LS10, Carl Zeiss Ltd., Nanterre, France) equipped with a five quadrants semi-conductor backscattered electron detector. The microscope was operated at 20 keV with a probe current of 250 pA and a working distance of 15 mm. The alveolar bone area located and imaged at a × 100 nominal magnification, corresponding to a pixel size of 1.1 μm per pixel. Four images per samples were taken, and the gray-level distribution of each image was analyzed with a lab-made routine in ImageJ. Three variables were obtained from the bone mineral density distribution: Ca_{peak} as the most frequently observed calcium concentration, Ca_{mean} as the average calcium concentration, and Ca_{width} as the width of the histogram at half maximum of the peak.

Furthermore, the elemental atomic bone composition was determined by energy-dispersive X-ray spectroscopy (EDS) with a 20 mm^2 X-max detector (Oxford Instruments, Abingdon, UK) fitted in the SEM and the Inca software. The

Ca/P ratio was computerized as the atomic ratio between calcium and phosphorus percent.

Analysis of bone vascularization

Catheterism of the right common carotid artery was done using a 24G catheter (Introcan Safety®, BBraun, Melsungen, Germany) under a binocular microscope (Leica, Weitzlar, Germany) with microsurgical specific instrumentation. Ligature of the catheter was done with an 8/0 suture thread. Venotomy of the right internal jugular vein was done to ensure blood drainage. First, a vascular rinse was performed using 5 ml of heparinized saline (Héparine sodique, Panpharma, Fougères, France). A solution composed of 5% of gelatin and 95% of a commercial barium sulfate solution used for digestive X-ray analysis (Micropaque®, Guerbet, Roissy, France) was prepared by heating at 37 °C. Then, 4 ml of this warmed solution were injected through the catheter. Ligature of the right and left common carotid arteries and the right and left internal jugular veins were done so that the solution remains in the injected vessels. The injected animals were placed in a cold room (4 °C) for 24 h to allow hardening of the vascular injection fluid. Hemimandibles were then dissected, defleshed, and fixed in formalin until use.

Micro-CT examination was done as described for microvascular analysis [40]. Briefly, a first micro-CT acquisition was done as described above. Samples were then decalcified using a mixture composed of 4% of formic acid, 10% of formalin in distilled water, changed twice a day, during 6 days. Decalcified samples were then rinsed in tap water to remove acid remnants and kept in formalin until use. A second micro-CT was then performed with the same procedure except for the rotation step which was fixed at 0.10° to allow better detail identification. So, for each hemimandible, two stacks of 2D sections were obtained (undecalcified and decalcified samples) and reconstructed using NRecon software (Bruker). 3D vascular reconstructions were obtained using VG Studio MAX 2.1 software (Volume Graphics GmbH, Heidelberg, Germany). 3D vascular volume of the alveolar bone (VV/TV_{ALV}, in %) was measured using CTAn software (Bruker). The reference volume of alveolar bone tissue TV_{ALV} was selected by a routine facility of the software after overimposing the 3D model obtained on the 1st scan prior to decalcification to the 2nd scan of the decalcified mandible. Technical details have been described previously [40].

Statistical analysis

Statistical analysis was performed using the Systat statistical software release 13.0 (Systat Software Inc., San Jose, CA). All data were expressed as mean ± standard error of the mean (SEM). Differences between groups were analyzed by a non-parametric test (Kruskall-Wallis). Differences were considered significant when $p < 0.05$.

Results

Animal loss and body weight

Eight rats died before sacrifice: three in the CTRL group and five in the ZA group. One rat died after an intravenous injection of ZA, seven rats died during the surgical procedure. In each group, the remaining rats were randomized in two subgroups: subgroup A and subgroup B (Fig. 1).

All rats gained weight during all time period of the study. Weight gain was 9.8 ± 0.7 g per week (12.5 ± 1.6 g for the CTRL group and 8.7 ± 0.7 g for the ZA group). A weight loss occurred during the 2 weeks following the tooth extraction procedure. The average weight loss was − 12.6 ± 2.2 g (i.e., − 2.16% of pre-extraction weight) with − 19.7 ± 5.8 g for the CTRL group and − 10.1 ± 1.8 g for the ZA group. No statistical difference was found between groups for any of these parameters at any time.

Macroscopic examination

Fifty-five percent of ZA-treated rats had an impaired healing with BRONJ lesions, consisting in mucosal ulcerations with large bone exposures, at the teeth extraction site (Fig. 2). No exposed mandibular bone was found in other locations. Normal wound healing with intact overlying mucosa and no bone exposure was observed in all rats of the CTRL group.

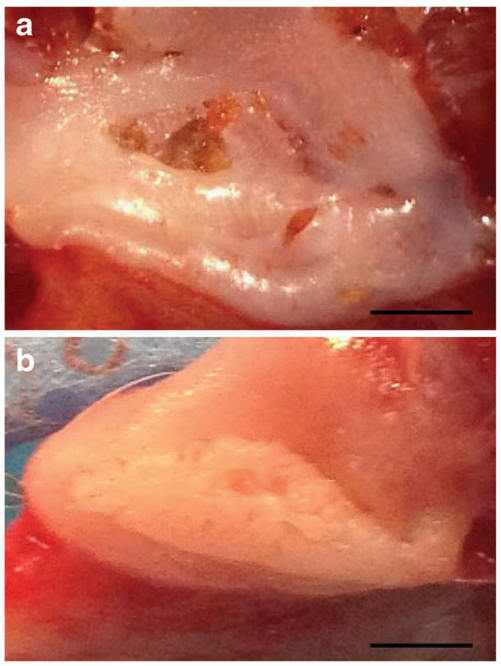

Fig. 2 Macroscopic aspects of extraction sites after sacrifice showing bone exposure in a ZA-treated rat (**a**) and normal wound healing with no bone exposure in a CTRL rat (**b**). The scale bars stand for 2 mm

Micro-CT analysis

Micro-CT analysis revealed typical signs of BRONJ: cortical osteolysis ($n = 9$), periosteal reaction ($n = 4$), and bone sequestration ($n = 2$) at the right molar area in rats of the ZA_A group ($n = 11$). 2D sections were obtained by a virtual cutting plane passing through the socket of the first molar or horizontally to identify periosteal reaction and bone sequestration (Fig. 3). No signs of BRONJ were found on the left hemimandibles of the ZA_A group nor on the right and left hemimandibles of the CTRL group. Tooth root remnants were noticed in the extraction sockets.

Raman analysis

The averaged Raman spectra of control alveolar bone, ZA impregnated alveolar bone and ZA are shown in Fig. 4. No difference between the spectra of control bone and ZA impregnated bone could be evidenced. The imidazole ring characteristic of ZA was undetectable in ZA impregnated bone. Mineralization ratio was found significantly increased in the ZA_A group (Table 1). Other parameters derived from Raman spectra did not significantly differ between ZA_A and $CTRL_A$ animals.

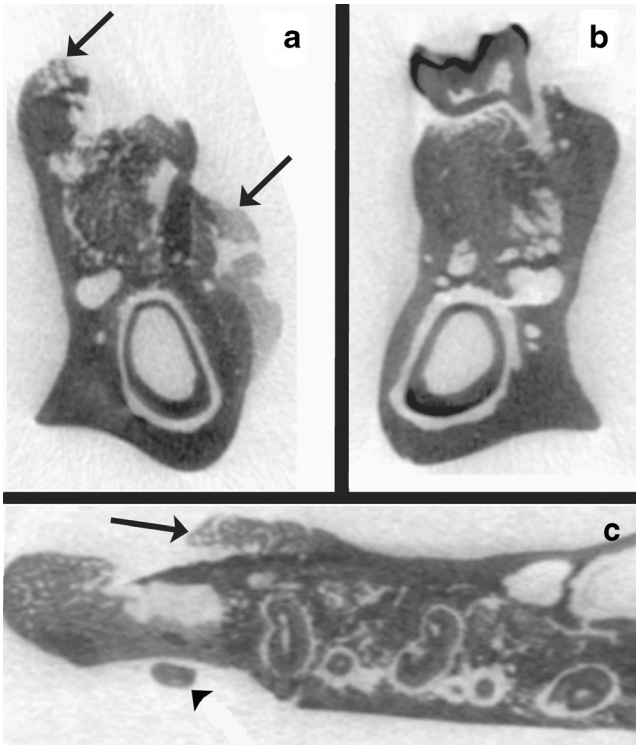

Fig. 3 Micro-CT analysis of alveolar bone modifications. 2D frontal sections of the right (**a**) and left (**b**) hemimandible of a rat of the ZA group. **c** 2D axial section of a right hemimandible of a rat of the ZA group showing periosteal reaction on the lingual side (black arrows) and bone sequestration (arrowhead) on the vestibular side. Tooth root remnants can be noticed in the extraction sockets

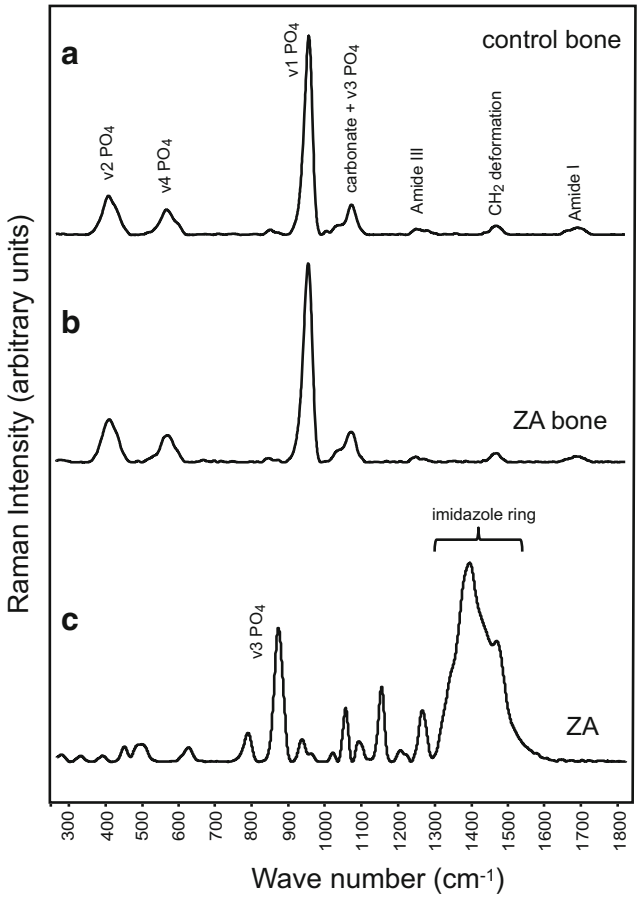

Fig. 4 Raman spectra of control alveolar bone (**a**), ZA impregnated alveolar bone (**b**), and dehydrated ZA (**c**). ZA spectrum is undetectable in the ZA impregnated bone

SEM-qBEI and EDS analysis

No significant differences were found for any of the qBEI parameters (Ca_{mean}, Ca_{peak}, and Ca_{width}) between ZA_A and $CTRL_A$ animals (Table 2). The Ca/P ratio did not significantly differ between the ZA_A and $CTRL_A$ groups.

Vascularization analysis

3D reconstructions of microvessels of alveolar bone were obtained (Fig. 5). The pedicle of the *nervus alveolaris inferior* was well seen and could be easily followed, the technique was also able to characterize the very thin capillaries in the alveolar region. On the 3D reconstructions, the vascular density seemed increased in the right hemimandible of $CTRL_B$ group after the tooth extraction. The vascular density also appeared reduced in the right hemimandibles of the ZA_B group, but no difference was noticed at naked eye on the 3D reconstructions between the density of the vascular bed on the left side of the CTRL and ZA animals. When VV/TV_{ALV} was measured, a significant difference was evidenced between the left and right side of the CTRL group (Fig. 6). A significant reduction of the

Table 1 Comparison between averages of spectroscopic parameters for each group after Raman analysis

	ZA	CTRL	*p*
Mineral/amide I	38.94 ± 1.40	32.94 ± 1.91	0.03
Mineral/amide III	72.10 ± 4.94	52.05 ± 4.70	0.02
Carbonate substitution	0.133 ± 0.002	0.131 ± 0.005	NS
Crystallinity	111×10^{-6}	111×10^{-6}	NS
PG content	0.198 ± 0.071	0.173 ± 0.043	NS

The gray boxes highlight a significant difference between ZA vs. CTRL

vascular bed was also evidenced when comparing the right side of the ZA_R and the $CTRL_R$ group.

Discussion

Clinically exposed bone is the main element of the clinical diagnosis of BRONJ in human. Our animal model's characteristics are close to those found in the literature [33, 35, 41–44]. The rat is the most used animal model for the development of bisphosphonates osteonecrosis of the jaw [33]. ZA doses used in the present study were very high (400 μg/kg per month) and are equivalent to those used in clinical practice for the treatment of myeloma in human [27, 45]. The use of high doses and long-lasting treatment are known to significantly increase the chance to develop BRONJ lesions [46]. We chose to use IV injection because it has the highest success rates in models of the literature and because it is similar to human clinic [42, 45, 47]. Tooth extraction was selected here as a triggering factor since BRONJ occurs after a tooth extraction in 60% of patients [15]. Similarly, we performed mandibular rather than maxillary tooth extraction, despite its difficulty, because BRONJ occurs more frequently at the mandible in 70% of the patients [48, 49]. Selected animals were free of

Table 2 qBEI and EDS parameters measured on the alveolar bone of the left hemimandibles

	ZA	CTRL	*p*
Ca_{peak} (%Ca)	18.57 ± 0.22	18.79 ± 0.34	NS
Ca_{mean} (%Ca)	18.1 ± 0.19	18.33 ± 0.3	NS
Ca_{width} (%Ca)	3.3 ± 0.13	3.32 ± 0.17	NS
Ca/P	1.423 ± 0.008	1.420 ± 0.018	NS

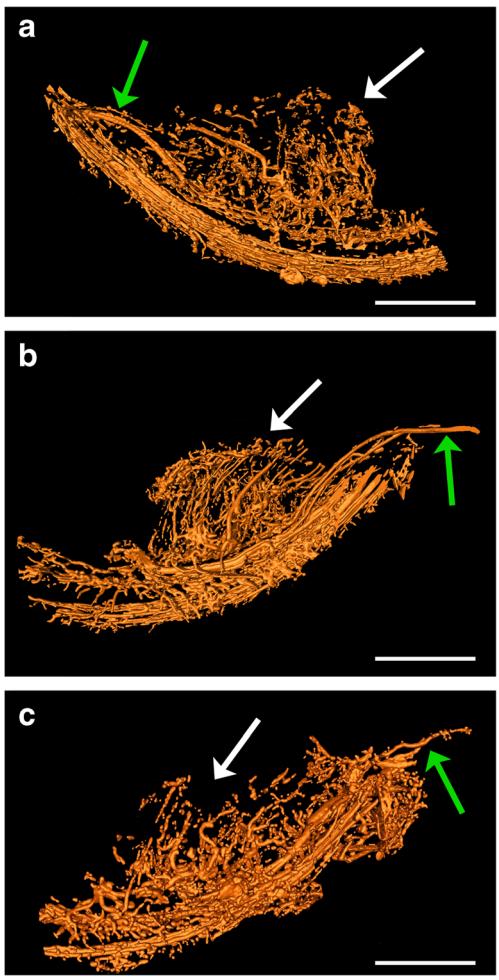

Fig. 5 **a** 3D micro-CT of the vascular bed in the molar areas of a left side of a CTRL rat. **b** Right side of a CTRL rat having had a molar extraction showing and increase in vessel density. **c** Right side of a ZA_A rat with a decreased vascular bed on the right side. White arrows show the alveolar areas. Green arrows show the vascular pedicle of the *nervus alveolaris inferior*. In all images, the scale bar stands for 4 mm

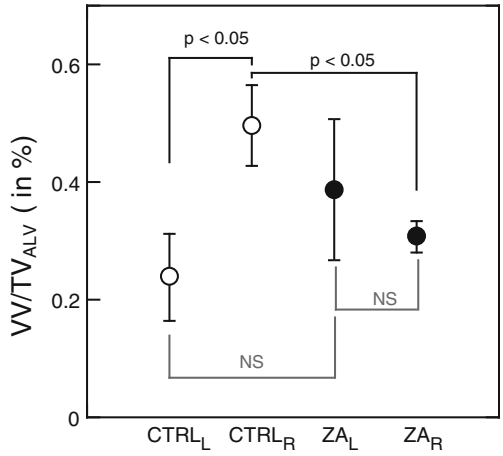

Fig. 6 3D vascular volume of the alveolar bone (VV/TV$_{ALV}$) for each group. CRTL rats (empty circles), ZA rats (filled circles). Significant and nonsignificant differences appear between each group

diseases for which zoledronic acid is administered in human (e.g., osteoporosis, myeloma, bone metastasis) and of other conditions, cofactors, coexisting systemic diseases, and concomitant medications. The aim was to avoid confounding factors and to demonstrate that BRONJ induction was only due to BPs. No additional drugs, such as dexamethasone and antibiotics, were given to animals. Additional drugs do not seem to give better results in BRONJ induction [33]. Macroscopic observations showed a bone exposure in 55% of the ZA treated animals and none in the control animals in the present study. Animal models aim at getting a high incidence of BRONJ: in the literature, varying rates of exposed bone are found in treated animals (0, 14, 33, 67, and 100%) and none in controls [33, 42, 45, 47, 50]. A recent review by Mitsimponas summarizes all animal models of BRONJ that have been developed [51]. However, bone exposure may be difficult to evidence because of its limited size and it should not be the only element to consider in assessing the quality of a BRONJ model. There was no significant weight difference between the two groups in the study. Only three comparable models in the literature report a statistical analysis of weight [41, 44, 52]. Weight is a parameter reflecting the animal welfare. Our results show that our model with tooth extraction and ZA has no negative impact on the animal.

In addition to clinical examination, micro-CT is used to assess the diagnosis of BRONJ in the rat since it provides 3D images and 2D reslicing in different planes. Numerous images of periosteal apposition and cortical erosion were found in ZA-treated rats. This has previously been reported in animal models of BRONJ [42, 53, 54]. Images of bone sequestration were also found in the present study as in human BRONJ [53].

Raman microspectroscopy aimed at investigating the presence of ZA in the bone matrix and to see the influence of this bisphosphonate on the mineral crystallinity. ZA was undetectable in the impregnated bone of ZA rats because the tissue concentration are very low [55]. In human bone sequesters from BRONJ patients, the characteristic bands of ZA could not be evidenced and an increase in the mineral to organic ratio was observed [56]. In another study, a decrease of crystallinity, determined with a 632 nm laser, was found in the newly formed bone in a calvaria defect in ZA-treated rats [57]. No change in crystallinity was found in the present study but the wavelength of our laser (785 nm) was different and another study reporting the Raman spectrum of ZA at 514 nm also show differences [58]. A SEM study with qBEI analysis found an increase in the calcium content of the bone matrix in animals treated during 3 years [59]. In the present study, this technique failed to identify similar changes, probably due to the shorter duration of the experiment. In a micro-CT experiment in ZA-treated rats treated up to 6 months, bone mineral density was found increased at the jaw [60]. Bone quality in rats treated with alendronate (another amino bisphosphonate) was found altered with an increased bone mineral density [61].

Analysis of the microvascularization showed that tooth extraction in CTRL animals increased vascularization in the mandibular alveolar bone. An increased capillary ingrowth is a normal reaction following tooth extraction [62]. ZA administration impaired this reactional increased vascular volume on the right side of ZA$_A$ rats. In vitro antiangiogenic effects of BP have been reported in several publications [26, 63, 64]. Some animal or human studies have found that BPs decrease the microvessel density and circulating endothelial cells and angiogenesis [25, 27–29, 47, 65–67]. This is the first study that analyzed bone microvascular bed in an animal model of BRONJ by vascular opacification and micro-CT.

In the present study, an impaired jaw bone vascularization due to an in vivo antiangiogenic effect of BPs was evidenced. The hypothesis of an inhibition of angiogenesis due to BPs in the pathophysiology of BRONJ is thus reinforced. Moreover, a significant increase of mineralization was found in the alveolar bone of ZA rats. This fact is in line with the pathophysiological hypothesis of altered bone quality with an increased stiffness of the bone matrix, due to a uniformity of the mineralization degree. The precise role of other pathophysiological hypotheses is still to be studied: direct toxicity of BPs for epithelial cells [31], reduced microcirculation of the gingiva, influence of BPs on immune cells leading to specific infections (*Actynomyces*) or osteomyelitis [22, 32]. A recent review summarizes all the currently advocated hypotheses [24].

In the present study, we aimed at provoking BRONJ in a rat model with mandibular tooth extraction. Clinical examination and micro-CT evidenced numerous signs of BRONJ. Our animal model of BRONJ has therefore some limitations. Mandibular molars extraction is not easy to perform since root remnants were observed. However, this created mandible osteonecrosis, a condition that reflects the human disease which is more frequently observed at the mandible. The

clinical and radiographic success rates obtained were lower than expected but fitted in well with similar studies reported in the literature.

Conclusion

The animal model described in the present study includes many elements of micro-CT diagnosis of BRONJ that are similar to what is found in computed tomography in human BRONJ [68]. Raman spectroscopy evidenced an increased mineral to matrix ratio in the alveolar bone after a prolonged treatment with ZA. SEM-qBEI evidenced no increase in the calcium content of the bone matrix in treated rats. Vascularization was increased after tooth extraction in the alveolar bone of control animals but was impaired by zoledronic acid in the same location in treated rats.

Acknowledgments The authors thank Mrs. N. Retailleau and S. Lemière for micro-CT. This work was made possible by funding from the French Minister of Research. Authors are greatly indebted to the SCAHU (Service commun d'animalerie hospitalo-universitaire) of Angers, especially to P. Legras and J. Roux for their help with the animal care.

Author contributions Jean-Daniel KÜN-DARBOIS performed animal handling, zoledronic acid injections, teeth extractions, and wrote the paper. Hélène LIBOUBAN performed animal handling and zoledronic acid injections, Guillaume MABILLEAU performed the SEM-qBEI analysis, Florence PASCARETTI performed Raman analysis, and Daniel CHAPPARD designed the study, performed micro-CT analysis, and wrote parts of the manuscript.

Compliance with ethical standards

Conflict of interest The authors declare that they have no conflicts of interest

Ethical approval All procedures performed in the present study were in accordance with the ethical standards of the institutional and national research committee and with the 1964 Helsinki Declaration and its later amendments. This experimental protocol was approved by the local ethical committee of Angers University Hospital (France) and was done in accordance with the institutional guidelines of the French Ethical Committee (protocol number 2016-31).

References

1. Russell RGG (2011) Bisphosphonates: the first 40 years. Bone 49: 2–19
2. Harrington JT, Ste-Marie LG, Brandi ML, Civitelli R, Fardellone P, Grauer A, Barton I, Boonen S (2004) Risedronate rapidly reduces the risk for nonvertebral fractures in women with postmenopausal osteoporosis. Calcif Tissue Int 74:129–135
3. Pols HA, Felsenberg D, Hanley DA et al (1999) Multinational, placebo-controlled, randomized trial of the effects of alendronate on bone density and fracture risk in postmenopausal women with low bone mass: results of the FOSIT study. Fosamax International Trial Study Group. Osteoporos Int 9:461–468
4. Terpos E (2012) Bisphosphonate anticancer activity in multiple myeloma. Anti Cancer Agents Med Chem 12:123–128
5. Musto P, Petrucci MT, Bringhen S et al (2008) A multicenter, randomized clinical trial comparing zoledronic acid versus observation in patients with asymptomatic myeloma. Cancer 113:1588–1595
6. Wang J, Goodger NM, Pogrel MA (2003) Osteonecrosis of the jaws associated with cancer chemotherapy. J Oral Maxillofac Surg 61: 1104–1107
7. Marx RE (2003) Pamidronate (Aredia) and zoledronate (Zometa) induced avascular necrosis of the jaws: a growing epidemic. J Oral Maxillofac Surg 61:1115–1117
8. Rachner TD, Platzbecker U, Felsenberg D, Hofbauer LC (2013) Osteonecrosis of the jaw after osteoporosis therapy with denosumab following long-term bisphosphonate therapy. Mayo Clin Proc 88:418–419
9. Ruggiero S (2014) Osteonecrosis of the jaw: BRONJ and ARONJ. Fac Dent J 5:90–93
10. Ruggiero SL, Dodson TB, Assael LA, Landesberg R, Marx RE, Mehrotra B, Task Force on Bisphosphonate-Related Osteonecrosis of the Jaws AAoOMS (2009) American Association of Oral and Maxillofacial Surgeons position paper on bisphosphonate-related osteonecrosis of the jaw - 2009 update. Aust Endodont J 35:119–130
11. Ruggiero SL, Mehrotra B (2009) Bisphosphonate-related osteonecrosis of the jaw: diagnosis, prevention, and management. Annu Rev Med 60:85–96
12. Vahtsevanos K, Kyrgidis A, Verrou E et al (2009) Longitudinal cohort study of risk factors in cancer patients of bisphosphonate-related osteonecrosis of the jaw. J Clin Oncol 27:5356–5362
13. Walter C, Al-Nawas B, Frickhofen N, Gamm H, Beck J, Reinsch L, Blum C, Grotz KA, Wagner W (2010) Prevalence of bisphosphonate associated osteonecrosis of the jaws in multiple myeloma patients. Head Face Med 6:11
14. Migliorati CA, Woo SB, Hewson I, Barasch A, Elting LS, Spijkervet FK, Brennan MT (2010) A systematic review of bisphosphonate osteonecrosis (BON) in cancer. Supp Care Cancer 18:1099–1106
15. Woo SB, Hellstein JW, Kalmar JR (2006) Narrative [corrected] review: bisphosphonates and osteonecrosis of the jaws. Ann Intern Med 144:753–761
16. Marx RE, Cillo JE Jr, Ulloa JJ (2007) Oral bisphosphonate-induced osteonecrosis: risk factors, prediction of risk using serum CTX testing, prevention, and treatment. J Oral Maxillofac Surg 65: 2397–2410
17. Marx RE, Sawatari Y, Fortin M, Broumand V (2005) Bisphosphonate-induced exposed bone (osteonecrosis/osteopetrosis) of the jaws: risk factors, recognition, prevention, and treatment. J Oral Maxillofac Surg 63:1567–1575
18. Boonyapakorn T, Schirmer I, Reichart PA, Sturm I, Massenkeil G (2008) Bisphosphonate-induced osteonecrosis of the jaws: prospective study of 80 patients with multiple myeloma and other malignancies. Oral Oncol 44:857–869
19. Diz P, Scully C, Sanz M (2013) Dental implants in the medically compromised patient. J Dent 41:195–206
20. Kwon T-G, Lee C-O, Park J-W, Choi S-Y, Rijal G, Shin H-I (2014) Osteonecrosis associated with dental implants in patients undergoing bisphosphonate treatment. Clin Oral Implants Res 25:632–640
21. Ata-Ali J, Ata-Ali F, Peñarrocha-Oltra D, Galindo-Moreno P (2016) What is the impact of bisphosphonate therapy upon dental implant survival? A systematic review and meta-analysis. Clin Oral Implants Res 27:e38–e46
22. Rasmusson L, Abtahi J (2014) Bisphosphonate associated osteonecrosis of the jaw: an update on pathophysiology, risk factors, and treatment. Int J Dent 2014:471035
23. Cardemil C, Thomsen P, Larsson Wexell C (2015) Jaw bone samples from bisphosphonate-treated patients: a pilot cohort study. Clin Implant Dent Relat Res 17(Suppl 2):e679–e691

24. Voss PJ, Poxleitner P, Schmelzeisen R, Stricker A, Semper-Hogg W (2017) Update MRONJ and perspectives of its treatment. J Stomatol Oral Maxillofac Surg 118:232–235
25. Pabst AM, Ziebart T, Ackermann M, Konerding MA, Walter C (2014) Bisphosphonates' antiangiogenic potency in the development of bisphosphonate-associated osteonecrosis of the jaws: influence on microvessel sprouting in an in vivo 3D Matrigel assay. Clin Oral Invest 18:1015–1022
26. Petcu EB, Ivanovski S, Wright RG, Slevin M, Miroiu RI, Brinzaniuc K (2012) Bisphosphonate-related osteonecrosis of jaw (BRONJ): an anti-angiogenic side-effect? Diagn Pathol 7:78
27. Sharma D, Ivanovski S, Slevin M, Hamlet S, Pop TS, Brinzaniuc K, Petcu EB, Miroiu RI (2013) Bisphosphonate-related osteonecrosis of jaw (BRONJ): diagnostic criteria and possible pathogenic mechanisms of an unexpected anti-angiogenic side effect. Vascular cell 5:1
28. Wehrhan F, Stockmann P, Nkenke E, Schlegel KA, Guentsch A, Wehrhan T, Neukam FW, Amann K (2011) Differential impairment of vascularization and angiogenesis in bisphosphonate-associated osteonecrosis of the jaw-related mucoperiosteal tissue. Oral Surg Oral Med Oral Pathol Oral Radiol Endod 112:216–221
29. Stresing V, Fournier PG, Bellahcene A, Benzaid I, Monkkonen H, Colombel M, Ebetino FH, Castronovo V, Clezardin P (2011) Nitrogen-containing bisphosphonates can inhibit angiogenesis in vivo without the involvement of farnesyl pyrophosphate synthase. Bone 48:259–266
30. Im G-I, Jeong S-H (2015) Pathogenesis, management and prevention of atypical femoral fractures. J Bone Metab 22:1–8
31. Reid IR, Bolland MJ, Grey AB (2007) Is bisphosphonate-associated osteonecrosis of the jaw caused by soft tissue toxicity? Bone 41:318–320
32. Russmueller G, Seemann R, Weiss K, Stadler V, Speiss M, Perisanidis C, Fuereder T, Willinger B, Sulzbacher I, Steininger C (2016) The association of medication-related osteonecrosis of the jaw with Actinomyces spp. infection. Sci Rep 6:31604
33. Sharma D, Hamlet S, Petcu E, Ivanovski S (2013) Animal models for bisphosphonate-related osteonecrosis of the jaws—an appraisal. Oral Dis 19:747–754
34. Sarkarat F, Kalantar Motamedi MH, Jahanbani J, Sepehri D, Kahali R, Nematollahi Z (2014) Platelet-rich plasma in treatment of zoledronic acid-induced bisphosphonate-related osteonecrosis of the jaws. Trauma Mon 19:e17196
35. Tsurushima H, Kokuryo S, Sakaguchi O, Tanaka J, Tominaga K (2013) Bacterial promotion of bisphosphonate-induced osteonecrosis in Wistar rats. Int J Oral Maxillofac Surg 42: 1481–1487
36. Li CL, Lu WW, Seneviratne CJ, Leung WK, Zwahlen RA, Zheng LW (2016) Role of periodontal disease in bisphosphonate-related osteonecrosis of the jaws in ovariectomized rats. Clin Oral Implants Res 27:1–6
37. Akkus O, Polyakova-Akkus A, Adar F, Schaffler MB (2003) Aging of microstructural compartments in human compact bone. J Bone Miner Res 18:1012–1019
38. Roschger P, Fratzl P, Eschberger J, Klaushofer K (1998) Validation of quantitative backscattered electron imaging for the measurement of mineral density distribution in human bone biopsies. Bone 23: 319–326
39. Mabilleau G, Mieczkowska A, Libouban H, Simon Y, Audran M, Chappard D (2015) Comparison between quantitative X-ray imaging, dual energy X-ray absorptiometry and microCT in the assessment of bone mineral density in disuse-induced bone loss. J Musculoskel Neuronal Interact 15:42–52
40. Nyangoga H, Mercier P, Libouban H, Basle MF, Chappard D (2011) Three-dimensional characterization of the vascular bed in bone metastasis of the rat by microcomputed tomography (MicroCT). PLoSOne 6:e17336
41. Abtahi J, Agholme F, Aspenberg P (2013) Prevention of osteonecrosis of the jaw by mucoperiosteal coverage in a rat model. Int J Oral Maxillofac Surg 42:632–636
42. Pautke C, Kreutzer K, Weitz J, Knodler M, Munzel D, Wexel G, Otto S, Hapfelmeier A, Sturzenbaum S, Tischer T (2012) Bisphosphonate related osteonecrosis of the jaw: A minipig large animal model. Bone 51:592–599
43. Marino KL, Zakhary I, Abdelsayed RA, Carter JA, O'Neill JC, Khashaba RM, Elsalanty M, Stevens MR, Borke JL (2012) Development of a rat model of bisphosphonate-related osteonecrosis of the jaw (BRONJ). J Oral Implantol 38 Spec No: 511–518
44. Abtahi J, Agholme F, Sandberg O, Aspenberg P (2012) Bisphosphonate-induced osteonecrosis of the jaw in a rat model arises first after the bone has become exposed. No primary necrosis in unexposed bone. J Oral Pathol Med 41:494–499
45. Biasotto M, Chiandussi S, Zacchigna S et al (2010) A novel animal model to study non-spontaneous bisphosphonates osteonecrosis of jaw. J Oral Pathol Med 39:390–396
46. Hoff AO, Toth BB, Altundag K et al (2008) Frequency and risk factors associated with osteonecrosis of the jaw in cancer patients treated with intravenous bisphosphonates. J Bone Miner Res 23: 826–836
47. Aguirre JI, Akhter MP, Kimmel DB, Pingel JE, Williams A, Jorgensen M, Kesavalu L, Wronski TJ (2012) Oncologic doses of zoledronic acid induce osteonecrosis of the jaw-like lesions in rice rats (Oryzomys palustris) with periodontitis. J Bone Miner Res 27: 2130–2143
48. Mavrokokki T, Cheng A, Stein B, Goss A (2007) Nature and frequency of bisphosphonate-associated osteonecrosis of the jaws in Australia. J Oral Maxillofac Surg 65:415–423
49. Bamias A, Kastritis E, Bamia C et al (2005) Osteonecrosis of the jaw in cancer after treatment with bisphosphonates: incidence and risk factors. J Clin Oncol 23:8580–8587
50. Hokugo A, Christensen R, Chung EM, Sung EC, Felsenfeld AL, Sayre JW, Garrett N, Adams JS, Nishimura I (2010) Increased prevalence of bisphosphonate-related osteonecrosis of the jaw with vitamin D deficiency in rats. J Bone Miner Res 25:1337–1349
51. Mitsimponas K, Moest T, Iliopoulos C, Rueger T, Mueller C, Lutz R, Shakib K, Neukam F, Schlegel K (2016) Search for a reliable model for bisphosphonate-related osteonecrosis of the jaw: establishment of a model in pigs and description of its histomorphometric characteristics. Br J Oral Maxillofac Surg 54:883–888
52. Ersan N, van Ruijven LJ, Bronckers AL, Olgac V, Ilguy D, Everts V (2013) Teriparatide and the treatment of bisphosphonate-related osteonecrosis of the jaw: a rat model. Dentomaxillofac Radiol 43: 20130144
53. Aghaloo TL, Kang B, Sung EC, Shoff M, Ronconi M, Gotcher JE, Bezouglaia O, Dry SM, Tetradis S (2011) Periodontal disease and bisphosphonates induce osteonecrosis of the jaws in the rat. J Bone Miner Res 26:1871–1882
54. Pacheco VN, Langie R, Etges A, Ponzoni D, Puricelli E (2015) Nitrogen-containing bisphosphonate therapy: assessment of the alveolar bone structure in rats—a blind randomized controlled trial. Int J Exp Pathol 96:255–260
55. Russell RGG, Watts NB, Ebetino FH, Rogers MJ (2008) Mechanisms of action of bisphosphonates: similarities and differences and their potential influence on clinical efficacy. Osteoporos Int 19:733–759
56. Juillard A, Falgayrac G, Cortet B, Vieillard M-H, Azaroual N, Hornez J-C, Penel G (2010) Molecular interactions between zoledronic acid and bone: an in vitro Raman microspectroscopic study. Bone 47:895–904

57. Olejnik C, Falgayrac G, During A, Cortet B, Penel G (2016) Doses effects of zoledronic acid on mineral apatite and collagen quality of newly-formed bone in the rat's calvaria defect. Bone 89:32–39
58. Boanini E, Gazzano M, Bigi A (2012) Time course of zoledronate interaction with hydroxyapatite nanocrystals. J Phys Chem C 116: 15812–15818
59. Misof BM, Roschger P, Gabriel D, Paschalis EP, Eriksen EF, Recker RR, Gasser JA, Klaushofer K (2013) Annual intravenous zoledronic acid for three years increased cancellous bone matrix mineralization beyond normal values in the HORIZON biopsy cohort. J Bone Miner Res 28:442–448
60. Vermeer J, Renders G, Duin M, Jansen I, Bakker L, Kroon S, Vries T, Everts V (2017) Bone-site-specific responses to zoledronic acid. Oral Dis 23:126–133
61. Verzola MHA, Frizzera F, de Oliveira GJPL, Pereira RMR, Rodrigues-Filho UP, Nonaka KO, Orrico SRP (2015) Effects of the long-term administration of alendronate on the mechanical properties of the basal bone and on osseointegration. Clin Oral Implants Res 26:1466–1475
62. Huebsch RF, Coleman RD, Frandsen AM, Becks H (1952) The healing process following molar extraction. I. Normal male rats (long-evans strain). Oral Surg Oral Med Oral Pathol 5:864–876
63. Fournier P, Boissier S, Filleur S, Guglielmi J, Cabon F, Colombel M, Clezardin P (2002) Bisphosphonates inhibit angiogenesis in vitro and testosterone-stimulated vascular regrowth in the ventral prostate in castrated rats. Cancer Res 62:6538–6544
64. Tang X, Zhang Q, Shi S, Yen Y, Li X, Zhang Y, Zhou K, Le AD (2010) Bisphosphonates suppress insulin-like growth factor 1-induced angiogenesis via the HIF-1alpha/VEGF signaling pathways in human breast cancer cells. Int J Cancer 126:90–103
65. Allegra A, Alonci A, Penna G et al (2010) Bisphosphonates induce apoptosis of circulating endothelial cells in multiple myeloma patients and in subjects with bisphosphonate-induced osteonecrosis of the jaws. Acta Haematol 124:79–85
66. Allegra A, Oteri G, Nastro E et al (2007) Patients with bisphosphonates-associated osteonecrosis of the jaw have reduced circulating endothelial cells. Hematol Oncol 25:164–169
67. Bi Y, Gao Y, Ehirchiou D, Cao C, Kikuiri T, Le A, Shi S, Zhang L (2010) Bisphosphonates cause osteonecrosis of the jaw-like disease in mice. Am J Pathol 177:280–290
68. Sigua-Rodriguez EA, da Costa RR, de Brito AC, Alvarez-Pinzon N, de Albergaria-Barbosa JR (2014) Bisphosphonate-related osteonecrosis of the jaw: a review of the literature. Int J Dent 2014:192320